IRSTI 47.45.00 https://doi.org/10.26577/phst20261318

The reduced size quasi-Yagi antenna with an ends-fed dipole-like driver

V. Atuchin[1,2,3*], D. Buhtiyarov[4], A. Gorbachev[3], V. Khrustalev[3] and N. Tarasenko[3]

[1]Kemerovo State University, Kemerovo, Russia
[2]Institute of Semiconductor Physics, SB RAS, Novosibirsk, Russia
[3]Novosibirsk State Technical University, Novosibirsk, Russia
[4]Institute of Cosmic and Aviation Materials (NIICAM Co. Ltd.), Pereslavl-Zalessky, Russia
*e-mail: atuchin@isp.nsc.ru
(Received April 4, 2026; received in revised form May 20, 2026; accepted May 29, 2026)

A modified version of the printed quasi-Yagi antenna by using the so-called ends-fed dipole-like radiator is presented. In this radiator, the excitation nodes are placed on the far ends of the dipole metallic halves rather than on the adjacent ones. As a result, the current distribution along each of the radiator cylindrical/printed wire significantly differs from that related to the ordinary center-fed dipole. That is why the frequency behavior of the proposed radiator input impedance guarantees the nontraditional radiation properties. Additionally, this approach to the choice of the excitation nodes leads to the simplification of the printed-circuit-board (PCB) implementation. A printed prototype operating at 2.8 GHz is developed and tested. Since the area around the radiating arms is fully free from any conductors and dielectrics (except for the substrate itself), the proposed quasi-Yagi antenna is a good candidate to emit radiation of high polarization purity. The measured results revealed that such an antenna is able to reach an effective area reduction to 40% with the enhanced up to 10 dB front-to-back ratio without decreasing the bandwidth.

Keywords: printed-circuit-board radiators, induced electromotive force method, quasi-Yagi antenna, radiation pattern, telecommunication.

1. Introduction

Modern wireless communication systems need wideband devices to transmit and receive simultaneously the signals with an acceptable isolation between transmitting and receiving channels [1]. To achieve this purpose, the development and improvement of printed directional antennas of various kinds remain topical [2]. A suppression of an unwanted radio frequency emission has led to an increasing demand for antennas, such as quasi-Yagi assemblies. There are many Yagi-Uda/quasi-Yagi antennas with a strip/coaxial feed and a dipole driver that have been presented for the last ten years [3-10]. Each of these antennas is a successful discovery in terms of its bandwidth, radiation patterns, size reduction and simple manufacturing. However, all the antennas contain a balance unit (balun) that is used to excite the center-fed dipole driver. Frequently, 180º out-of-phase balun nodes are displaced in the area substantially, and that increases the surroundings around the dipole nodes and affects the polarization purity of radiation. This also needs an accurate accomplishment of design, including the line length, as well as its meandering/turning. The difficulties mentioned bring some sort of motivation for a further investigation of quasi-Yagi antennas. Below, we describe a novel modification of the printed ones.

This approach is based on the utilization of the so-called "end-fed dipole radiator" (EFDR) patented in [11] and then successfully used in [12] to improve the one-band quasi-Yagi antenna. Lately, this EFDR was realized for the waveguide excitation [13] and was used in the printed dual-band quasi-Yagi antenna on the base of the broadband balun with microstrip-to-slotline transitions [14]. The architecture, which is described below, is the result of an attempt to alleviate the complication of a coaxial/strip feed with a regular wire antenna design principle by combining the nonstandard ends-fed dipole-like radiator and a balun that is implemented on a base of the microstrip-slot and parallel stripline-microstrip transitions. A systematic study of the modified printed quasi-Yagi antenna is briefly presented, and the following numerical optimization of the proposed antenna by a proper 3D EM solver is described. As a result, all the key geometrical dimensions were established and then successfully used through the PCB fabrication on the standard Cu-clad dielectric substrate FAF-4D (Russia) with the 1.5 mm thickness. The simulation-derived and anechoic chamber-based experimental results are used to verify the described approach. The slight difference between the numerical and experimental values may be caused by the round corners of the strip-line topology as well as the discontinuity of the coaxial adapter, manufacturing imperfections and radio frequency interconnections by using a coaxial cable. These features were not taken into account through the full-wave simulation. The use of such a driver contributes to an increase in the degree of freedom in the design of printed quasi-Yagi antennas. At the same time, depending on the set of requirements of the tactical and technical specifications for the design, various optimization strategies can be constructed.

2. Current distribution along the stand-alone EFDR and its radiation resistance

As proposed in [11], an ends-fed dipole-like radiator contains two thin $(a \ll l)$ collinear cylindrical wires 1 and 2, an energized coaxial cable 3 and the balance unit (balun) 4 having the input port 5 and 180º out-of-phase output ports 6 and 7 (Figure 1(a)). The adjacent ends 8 and 9 of both wires are placed in the immediate nearness ($b \ll l$), whereas the far ends of those play the role of the input terminals 10 and 11.

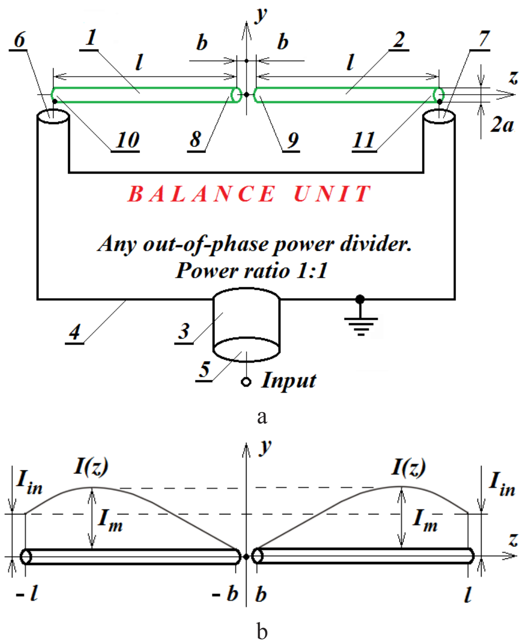

Figure 1. Stand-alone ends-fed dipole-like radiator: (a) functional scheme, (b) current distribution along the wires.

Now, the detailed analysis described in [15] leads to the following expressions for the current distribution $I(z)$ along the wires (Figure 1(b)) and for EFDR radiation resistance R_{rad}:

$$I(z)=\begin{cases} I_m \sin(+kz), 0<z\le +l, \\ I_m \sin(-kz), -l\le z<0. \end{cases}$$

$$R_{rad}=2P_{rad}\Big/\left|I_m\right|^2=60\int_0^{\pi}\left[Q^2\Big/\sin\theta\right]d\theta$$

$$=30\left\{3\gamma+\ln\left[4(kl)^3\right]+Ci(4kl)-4Ci(2kl)+2\sin\left[(kl)^2\right]\left[\frac{\sin(2kl)}{2kl}-1\right]\right\}, \quad (1)$$

where P_{rad} represents the total power radiated from the EFDR through the closed sphere lying around a radiator in the far-field Fraunhofer region, I_m is the current maximum, k = 2π/λ, λ is the free space wavelength, γ = 0.5772157 (Euler constant), $Ci(x)$ is the cosine integral, and the quantity Q is determined as:

$$Q=1-\cos(kl\cos\theta)\cos(kl)-\sin(kl\cos\theta)\sin(kl)\cos\theta .$$

Now, according to [2, Chapter 8], the real part R_m of an input impedance $Z_m=R_m+jX_m$ referred to at the current maximum I_m can be expressed as $R_m=R_{rad}$, whereas the real part R_{in} of the input impedance $Z_{in}=R_{in}+jX_{in}$ referred to at the current I_{in} at the input terminals 10 and 11 (Figure 1(b)) can be obtained by a transfer relation $I_{in}=I_m\sin(kl)$, or:

$$R_{in}=R_m\Big/\sin^2(kl). \quad (2)$$

As may be seen, the current distribution $I(z)$ along the EFDR is significantly different from the distribution specific to a classical ordinary dipole radiator. Therefore, the frequency response of the input impedance of the EFDR considered will be significantly different from the similar frequency response of the classical dipole. This should be taken into account through the antenna design.

3. Self-impedance of the Stand-alone EFDR

As a result, the induced electromotive force (*emf*) method leads to closed-form solutions which provide such the design data that can be used directly as very good initial parameters in the full-wave 3D EM simulation. According to [15], both the real R_m [R_{in}] and the imaginary X_m [X_{in}] part of the self- [input] impedance $Z_m=R_m+jX_m$ referred to at the current maximum I_m [$Z_{in}=R_{in}+jX_{in}$ referred to at the current I_{in} at the input terminals 10 and 11] can be expressed for a free-space as (in Ohms):

$$R_m=60\left\{\sin^2(kl)\left(\frac{\sin(kl\sqrt{4+(a/l)^2})}{kl\sqrt{4+(a/l)^2}}-\frac{\sin(ka)}{ka}\right)+3Ci(ka)\right.$$

$$+0.5Ci[kl(\sqrt{4+(a/l)^2}+2)]+0.5Ci[kl(\sqrt{4+(a/l)^2}-2)]$$

$$\left.-2Ci[kl(\sqrt{1+(a/l)^2}+1)]-2Ci[kl(\sqrt{1+(a/l)^2}-1)]\right\} \quad (3)$$

$$X_m=60\left\{\sin^2(kl)\left(\frac{\cos(kl\sqrt{4+(a/l)^2})}{kl\sqrt{4+(a/l)^2}}-\frac{\cos(ka)}{ka}\right)-3Si(ka)\right.$$

$$-0.5Si[kl(\sqrt{4+(a/l)^2}+2)]-0.5Si[kl(\sqrt{4+(a/l)^2}-2)]$$

$$\left.+2Si[kl(\sqrt{1+(a/l)^2}+1)]+2Si[kl(\sqrt{1+(a/l)^2}-1)]\right\} \quad (4)$$

$$R_{in}=R_m\Big/\left[\sin(kl)\right]^2,\ X_{in}=X_m\Big/\left[\sin(kl)\right]^2. \quad (5)$$

The numerical analysis of the last relations indicates that the input impedance $Z_{in}=R_{in}+jX_{in}$ [quantities in (5)] is characterized by a significant capacitive component with a curvilinear change in l/λ within the range of $0.1<l/\lambda<0.6$. At the same time, the real part R_{in} [Ohm] changes in the range of $15 < R_{in} < 180$. These results are used in the following considerations related to the EFDR vertically placed above the ground.

The presence of an obstacle (such as a rectangular waveguide), especially in the vicinity of a radiating element, will significantly alter the overall radiative properties of the antenna system. In practice, the most common always considered obstacle is the ground. The energy radiated by the radiating element and oriented in the direction of the earth is reflected. The amount of reflected energy and its direction are dependent on the ground metallic geometries and their dimensions.

To analyze the behavior of the antenna near a ground conductor, virtual sources (source images) must be introduced to take reflections and interference into account [2]. As it follows from the name, these are not real sources, but imaginary ones, which, when combined with real sources, form an equivalent system. For the purposes of analysis only, the equivalent system gives the same radiated field on and over the conductor as the real system itself. Under the conductor, the equivalent system is not able to give the correct field. However, in this region, the field is equal to zero and equivalence is not needed. When the height of the source above the plane h is equal to zero, primary and secondary horizontal fields of an electric vibrator and a vertical magnetic vibrator become equal in terms of amplitude and opposite in sign, the total field becomes zero and the radiation disappears. Conversely, in the case of a vertical electric vibrator and horizontal magnetic vibrator, the primary and secondary fields at $h = 0$ become equal in amplitude and sign, so that the total field is doubled relative to the field of the same source in free space. Concerning the resistance and conductivity of radiation sources, then, at $h = 0$ in the first case, they become equal to zero, and, in the second, – they double. The doubling resistance and conductivity of radiation is related to the fact that the radiated power density in each point in space is quadrupled, but the energy is radiated only into the upper half-space.

4. Printed quasi-Yagi antenna employing microstrip-slot and stripline-microstrip transitions

The results indicated in the previous section are used here to create the proposed antenna topology. Contrary to the version on the base of the printed rectangular-coaxial (recta-coax) transmission line described in [15], it is useful to modify both the driver and director in order to realize the more compact strip-line architecture. To do so, the quarter-wave directional coupler should be omitted from the architecture described in [15], and then the compact planar out-of-phase power divider proposed in [16] will be used. As a result, after the use of equations (1) – (5) for the recalculation of the strip widths, two proper dielectric substrates with copper clothes are used simultaneously to realize the printed ends-fed driver, as well as the printed director and power divider without any metallized via-holes (Figure 2, all dimensions are in mm).

After calculations, it is necessary to refine and optimize the pieces of the topology in a specialized program of electrodynamic modeling. The optimization in the program is divided into several stages, at each of which certain antenna components or fragments of complex elements are optimized. For example, in the case of a multi-component Yagi antenna having a dipole-like driver, several directors and a reflector, the optimization process is carried out in three steps. Before a brief description of the optimization steps, it is useful to note that, in printed versions of Yagi antennas, the edge of a metallized rectangle plays the role of a reflector. Such use of the grounded fragment foil edge as a reflector was previously described in printed Yagi antennas [3], and it was successfully applied as a reflector of other quasi-Yagi antennas, including the described novel printed quasi-Yagi antenna with an ends-fed dipole-like driver. In the authors' opinion, it is quite difficult to compact describe the optimization process with references to formulas (1) – (5). The optimization process itself is based on trial-and-error and depends heavily on the experience of the project implementers. Therefore, what follows is a description of the optimization process as the authors see it.

In the first optimization step, the distance between the driver and the nearest elements is optimized directly, i.e., usually the edge of the fragment located on the back of the dielectric substrate. Also, the distance between the driver and the first passive element (director) is optimized at the first step. Initially, the calculated dimensions of the driver itself are determined by the parameters of the terms of reference and correspond to the selected working frequency. In this case, the distances between passive elements and their dimensions are set in the program with a spread of parameters of approximately 10-15%. This tolerance is quite enough to select the optimal dimensions of the antenna elements. At the first stage of optimization, it is desirable not to pay much attention to the shape of the radiation pattern, but to carry out the optimization itself in terms of the quality of antenna matching. Just this parameter, at the first stage, is the key and allows in the future, at the next steps, obtaining the necessary shape of the antenna pattern, as well as to reach the required gain.

At the second stage of optimization, distances between other directors are selected (if any). As the number of the directors increases, the antenna gain also increases, the beam pattern narrows, and the antenna becomes more directional. In other words, the optimization of a Yagi antenna with more than three directors is a long process involving many complex tasks, since it is necessary to control several parameters of the antenna (reflection coefficient, radiation pattern shape, gain) and at the same time ensure that the working frequency of the antenna remains unchanged. Additionally, with a large number of directors, in order to maintain the required characteristics, it is sometimes necessary to change the central location of passive elements, slightly shifting them from the central axis of the antenna in one direction or another. Also, the use of various types of drivers leads to a different distance between directors and to the width of passive elements.

At the third stage, the lengths and widths of the directors themselves are optimized. At this stage, the optimization is carried out on all necessary parameters and not only on the matching characteristic. At the same time, the center frequency of the antenna does not shift. And if the shape of the directional pattern does not meet the requirements of the terms of reference, in addition to changes in the third optimization step, it is necessary to make small changes in the director positions obtained in the previous step.

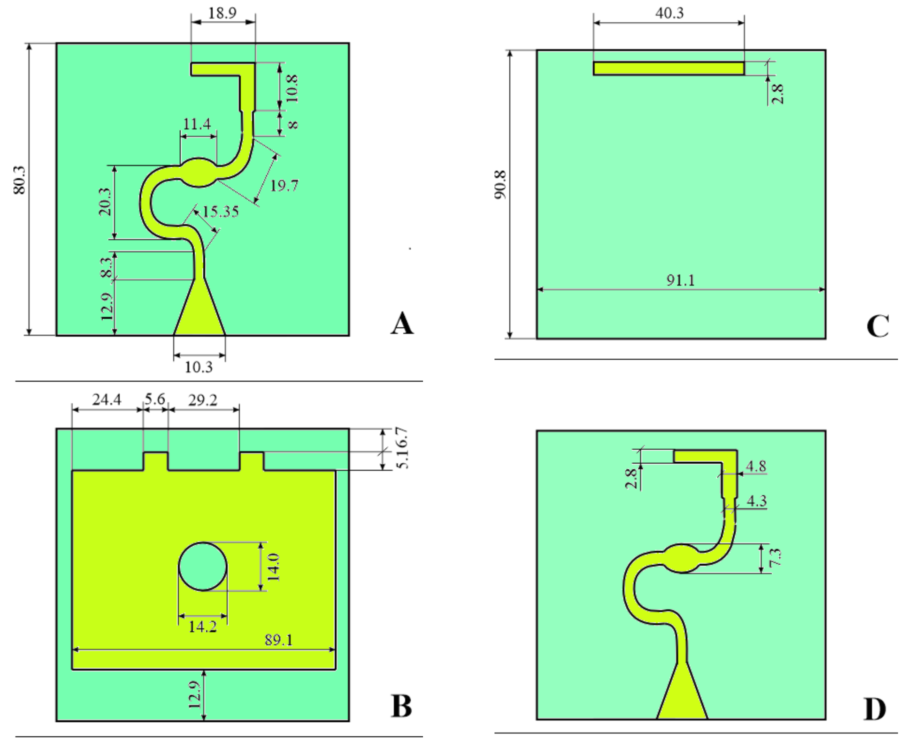

Figure 2. Three-layer printed-circuit-board implementation of the radiating domain and out-of-phase power splitter related to the modified version of the quasi-Yagi antenna employing only two dielectric substrates: (A) top side of the first substrate, (B) bottom one of that, (C) top side of the second substrate, and (D) bottom one of that.

In this modification, two Cu-clad dielectric sheets (Russia) are used. Namely, to realize the whole three-layer sandwich structure (Figure 2) related to both the radiating part of the quasi-Yagi antenna and the nonradiating domain containing the power divider itself, the 1.5 mm thick organic dielectric substrates FAF-4D (Russia) were used. This nomenclature was chosen because of its low loss tangent (tanδ = 0.002) and a small relative dielectric constant variation ($\varepsilon_r = 2.5 \pm 0.1$) [17]. The copper foil thickness is equal to 0.035 mm.

Without loss of generality, the center frequency of the proposed whole quasi-Yagi antenna was chosen to be 2.8 GHz. After the corresponding systemic design and nonlinear parametric optimization through the 3D full-wave solver "CST Studio Suite" [18], the final geometrical dimensions were found, as shown in Figure 2 (in mm). The printed-circuit-board implementation was performed using the conventional Russian photo-lithography procedure and wet etching.

As a result, the presented topology version of the planar quasi-Yagi antenna was measured on a base of the anechoic chamber by using an ordinary far-field measurement arrangement. The KRPG-434511.016 connector [19, Figure 3, Table 8] was used to connect the manufactured antenna (Fig. 3) with the measurement equipment. The impedance matching was investigated using an Agilent N5241A Performance Network Analyzer, whereas the antenna radiation patterns were established at the indoor far-field laboratory. The antenna-under-test was mounted on the rotating pedestal, and the standard linearly-polarized pyramidal horn was excited by an E8257D PSG microwave signal generator. Namely, the results related to the voltage standing wave ratio (VSWR) show the acceptable comparison (Figure 4). Some discrepancies are attributed to the impedance imperfections in the test equipment, including the soldering areas and attainable resolution of the wet etching.

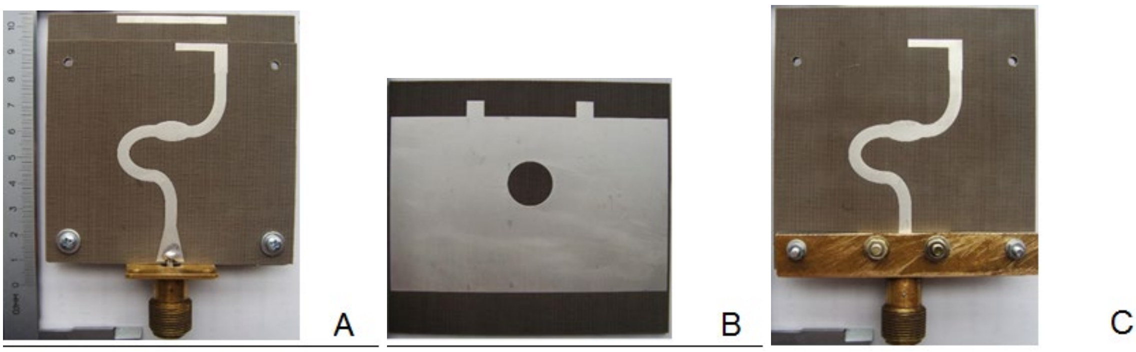

Figure 3. Photos of the proposed quasi-Yagi antenna: (A) face side, (B) the middle metallization realized on the bottom side of the first substrate, and (C) bottom side of the antenna.

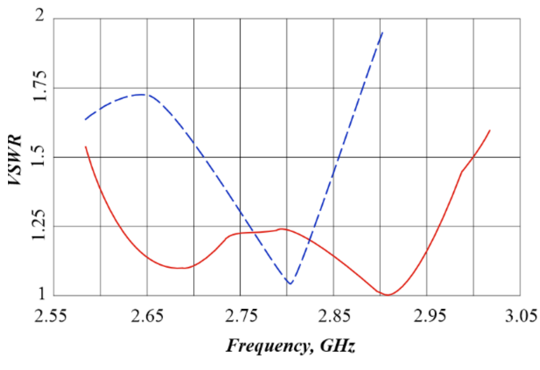

Figure 4. Simulated (- – -) and measured (—) VSWR of the proposed quasi-Yagi antenna.

As can be seen in Figure 4, the VSWR of the antenna at the 2.8 GHz center frequency is approximately 1.24. It can be noted that the experimentally obtained characteristic has its minima at frequencies 2.63 and 2.91 GHz, while the VSWR minimum value obtained from computer modeling is reached at the center frequency of the antenna 2.8 GHz. From the obtained data, it can be concluded that the change in the shape of the VSWR diagram after the implementation of the antenna is associated exclusively with the technological features of manufacture. Additionally, the parametric studies presented in Figs S10–S12 (please see the “Supporting information”) show that the input VSWR is extremely sensitive to the vertical dimensions of the elliptical patch (Dy_cop) and the vacuum hole (Dy_vac). This explains also the discrepancy in the measured VSWR (Fig. 4). Apparently, the manufacturing tolerances of these specific elements are the likely cause of the dual-resonance behavior in the experimental prototype. So, for example, the modeling does not take into account the attachment screws connecting the two substrates. In addition, it is likely that the attachment of the feed connector, the presence and location of solder have a great influence. A detailed analysis of the VSWR diagram is not beyond the scope of this study. However, it is useful to note that the radiation pattern of the implemented sample at the center frequency of 2.8 GHz, practically, coincides with the radiation pattern obtained by computer modeling. At frequencies where the experimental VSWR diagram reaches minimum values, the antenna pattern has a slightly different, yet acceptable, shape. As a result, the technological inaccuracies have led to an increase in the antenna bandwidth. That is, the VSWR of the antenna is less than 1.25 in a frequency band of approximately 0.4 GHz. This fact can be used to study the possibility of expanding the antenna working frequency band while maintaining all the necessary characteristics, such as radiation pattern shape and antenna gain. In general, it can be concluded that, in order to improve the quality of antenna matching at the center frequency, it is necessary to make changes in the antenna manufacturing process, namely, in the power connector installation. At the same time, even the current VSWR value meets the requirements for antennas used in telecommunication systems. The corresponding simulated current distributions on the surfaces of the modeled quasi-Yagi antenna at the selected three frequencies are presented in “Supporting information”. These figures confirm the proposed design based on the systematic parametric optimization. Additionally, the current distributions at the center frequency of 2.8 GHz are presented in Figure 5. This figure demonstrates the physical feasibility of the “ends-fed” concept. To improve the readability of the text, this figure is repeated in Figure S2 of the “Supporting information”. It should be also noted that the differences between simulation and measurements are due to two main groups of influencing factors. Specifically, the first group is caused by the manufacturing process of nonradiative microstrip-slot and parallel stripline-microstrip transitions that contain a number of curved fragments proposed in [16]. The second one is driven by the optimization strategy and accuracy, related to the antenna’s radiating part. This includes: lengths and widths of elongated linear conductors, as well as the distances between them and their arrangement on the antenna dielectric substrate. In this group, the manufacturing tolerances play a less prominent role due to the simplicity of implementing the elongated linear conductors.

Now, in Figure 6 are both the measured and simulation-derived E- and H-plane normalized radiation patterns at 2.8 GHz with a front-to-back ratio of approximately 9.8 dB. The simulated cross-polarization fields of the antenna exhibit almost omnidirectional patterns with the peak around -32 and -24 dB in the E– and H–planes, respectively, and they are not shown in the plots for brevity. The measured cross-polarization patterns are 7 dB larger than those produced through the simulation and they are also not shown here in the graphs for brevity. Thus, both the co-polarization patterns and the cross-polarization intensities have acceptable behaviors in the frequency range of interest. At the same time, the following parameters/indicators, related to the cross-polarization intensities, were implemented in previously published works [7], [9], [20], and [21], respectively:

- the maximum cross-polarization level in the E-plane is -15 dB [7], -20 dB [9], -18 dB [20], -19 dB [21];
- the maximum cross-polarization level in the H-plane is -12 dB [7], -15 dB [9], -14 dB [20], -15 dB [21].

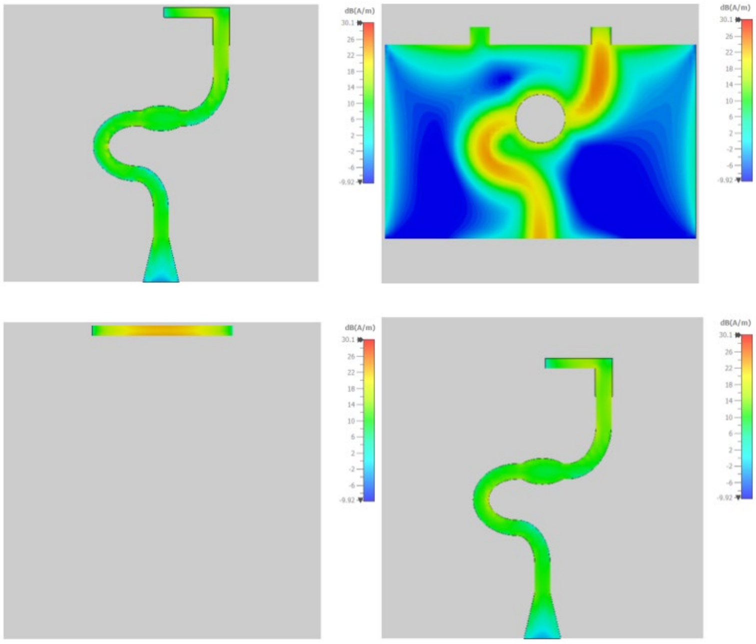

Figure 5. Simulated current distributions on the surfaces of all the layers at the frequency 2.8 GHz.

It is advisable to note that the use of two dielectric substrates noticeably complicates the antenna design. But on the other hand, this allows the implementation of an antenna with additional degrees of freedom through the design process. Additionally, the requirements of the structural and technological parameters are significantly weakened in the proposed antenna, and it is possible to assign bigger allowances to the geometric dimensions of printed strip conductors.

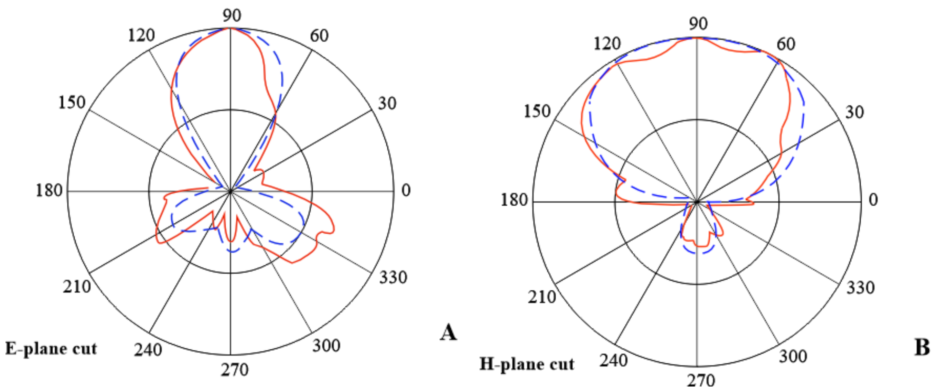

Figure 6. Simulated (- – -) and measured (—) radiation patterns: (A) E–plane, (B) H–plane.

As can be seen in Figure 6, the antenna beam width in the half power level in the E-plane cut is approximately 45 °, which is the optimal value required in the design of radio engineering systems. However, this beam width is slightly less than that obtained as a result of computer modeling, and also it turns out to be insignificantly shifted towards the left hemisphere. It is also worth noting that the radiation level in the lower hemisphere in this plane reaches sufficiently high values. It is possible to reduce the side lobes by including an additional number of directors in the antenna, as well as by implementing the antenna on one dielectric sheet, without using a second fragment on which the director is located in the antenna described above. One of the factors affecting the diagram is the presence of attachment screws connecting the two substrates. Thus, the implementation of an antenna on a single dielectric sheet will help to improve the shape of the radiation pattern and will probably lead to an improvement in the quality of antenna matching at the center frequency. Aligning the direction and shape of the main lobe of the antenna is likely to allow the director to move some distance in one or another direction relative to the central axis of the antenna. This goal was not set in the current work, and so it is not considered. The beam width in the H-plane cut is approximately 110°. At the same time, in the lower hemisphere, the maximum radiation level is characterized by acceptable values and turns out to be lower than the values obtained as a result of computer optimization, which is an acceptable indicator for most technical applications.

In general, the shape of the radiation pattern of the described antenna is acceptable for the use in various telecommunications systems. To the author knowledge and comprehension, contrary to the latest contributions [20], [21], [22], the proposed quasi-Yagi antenna is characterized by the acceptable radiation properties, as well as by the more compact architecture. This offers an additional degree of freedom through the PCB implementation. To be used in the systems that require a more narrow oriented diagram, as well as higher noise immunity and, as a result, a lower level of side lobes, it is necessary to modify the antenna by increasing the number of directors, changing the technical implementation (using one dielectric substrate instead of two), as well as more detailed optimization in the computer program.

The efficiency of the proposed antenna can be discussed as an analysis of the curves shown in Figures 4 and 6. As can be seen in Figure 4, the VSWR of the antenna at the 2.8 GHz center frequency is approximately 1.24. The VSWR of the antenna that was obtained after the 3D simulation is much better, and it is close to 1.05. It means that the antenna matching can be much better and can be improved by not using, for example, the attachment screws connecting the two substrates. As can be seen in Figure 6, the antenna beam width in the half power level in the E-plane cut is approximately 45°, which is the optimal value required in the design of radio engineering systems. The side lobes level is worse than the same one of the 3D simulation model. The efficiency can be increased, if this side lobe level is decreased. As it was pointed, one of the factors affecting the diagram is the presence of attachment screws connecting the two substrates. Thus, the implementation of an antenna on a single dielectric sheet would help to improve the radiation pattern shape and will also, probably, lead to an improvement in the quality of antenna matching at the center frequency. The parametric studies of the proposed antenna are of great significance, and the results are presented in Figures S1-S14 (Supporting materials). For example, Figure S7 shows that the E-plane pattern is rather sensitive to the director length. This confirms that the antenna's performance is tied to a very specific optimized state, reinforcing the need for high-precision PCB manufacturing in case of mass production. The obtained dependences indicate that the proposed quasi-Yagi antenna is characterized by appropriate properties and, accordingly, it can be used in compact printed antenna systems with linearly polarized radiation properties. It is worth noting that a more rigorous comparison between simulation and measurement results can be performed based, for example, on the approach presented in [24]. However, the referenced study utilized curved radiating sector-like antenna fragments. In contrast, the radiating fragments in the authors' study are simpler – elongated and linear – allowing for the application of more straightforward system-oriented optimization approaches.

5. Conclusion

A novel implementation of the printed quasi-Yagi antenna with end fire-like radiation and good polarization purity was proposed. To realize the necessary pattern, an ends-fed dipole-like radiator was briefly described for completeness. According to this description and by addition the corresponding mathematical expressions in closed forms established in [12], [13], the novel architecture of the quasi-Yagi antenna was proposed. Through this improvement, the systematic parametric optimization was successfully used in order to include the classical out-of-phase power divider in the design process [16]. This divider is very compact in the PCB implementation and acts as the necessary balance unit. The above-mentioned radiation properties make the antenna a qualitative standalone module or a suitable candidate for phased arrays. The antenna can be used as a single unit or as a part of phased array. Also it can be used as a radiator or as a driver element of the Yagi antenna with more than one director element. It should be noted once again that the proposed antenna employs an innovative dipole-like driver with ends-fed excitation [11]. Although it does not deliver breakthrough radiation performances compared to recent quasi-Yagi antenna designs [3 – 9], the use of this driver still increases the number of degrees of freedom when designing similar antennas. If any antenna system (e.g., phased array) needs an antenna beam width of about 30°, the antenna must contain more than two directors. If it is used in telecommunication systems, the antenna beam width can stand the same as that obtained in this work. An attractive feature of the described quasi-Yagi antenna is its compact size for microwave frequency band that paves a way for new applications in wireless communication systems. Apparently, the authors of other similar studies pursued the same goals. Works [23] and [24] can be cited as examples.

Funding

The research was carried out with financial support from the Russian Science Foundation within the framework of scientific project No. 24-29-20048, https://rscf.ru/project/24-29-20048/, as well as by the financial support from the Government of Novosibirsk region, agreement No. p-77.

Conflicts of interest

The authors declare no conflict of interest.

Author contributions

Conceptualization, A.G.; Data curation, V.K. and N.T.; Formal analysis, D.B. and N..T.; Investigation, V.A. and N.T.; Methodology, A.G.; Software, D.B.; Supervision, V.A.; Validation, V.A. and D.B.; Writing – original draft, A.G.; Writing – review & editing, N.T; Funding Acquisition, A.G.

References

1. Z. N. Chen, Editor. *Handbook of Antenna Technologies*, Singapore: Springer, 2016, Volume 3, Chapter VI.
2. C. A. Balanis, *Antenna Theory. Analysis and Design,* Hoboken, NJ: John Wiley & Sons, 2016, Chapters 2, and 5.
3. S.-J. Wu et al., “A multiband quasi-Yagi type antenna,” *IEEE Trans. Antennas Propag*., vol. 58, no. 2, 2010, pp. 593–596.
4. P.-Y. Qin et al., “Frequency reconfigurable quasi-Yagi folded dipole antenna,” *IEEE Trans. Antennas Propag*., vol. 58, no. 8, 2010, pp.2742–2747. https://doi.org/10.1109/TAP.2010.2050455
5. Y. Ding et al., “Design of a multiband quasi-Yagi-type antenna with CPW-to-CPS transition”, *IEEE Antennas Wireless Propag. Lett*., vol. 10, 2011, pp. 1120–1123. https://doi.org/10.1109/LAWP.2011.2170950
6. P.-Y. Qin et al., “A beam switching quasi-Yagi dipole antenna”, *IEEE Trans. Antennas Propag*., vol. 61, no. 10, 2013, pp. 4891–4899. https://doi.org/10.1109/TAP.2013.2274635
7. J. Wu et al., “Bandwidth enhancement of a planar printed quasi-Yagi antenna with size reduction”, *IEEE Trans. Antennas Propag*., vol. 62, no. 1, 2014, pp. 463–467. https://doi.org/10.1109/TAP.2013.2287286
8. Z. Liang et al., “A novel microstrip quasi Yagi array antenna with annular sector directors”, *IEEE Trans. Antennas Propag*., vol. 63, no. 10, 2015, pp. 4524–4529. https://doi.org/10.1109/TAP.2015.2456875
9. M.-C. Tang et al., “Flexible efficient quasi-Yagi printed uniplanar antenna”, *IEEE Trans. Antennas Propag*., vol. 63, no. 12, 2015, pp. 5343–5350. https://doi.org/10.1109/TAP.2015.2486807
10. A. P. Gorbachev et al., “Planar dual-frequency quasi-Yagi antenna”, *Electromagnetics*, vol. 36, no. 5, 2016, pp. 328–339.
11. D. A. Bukhtijarov et al., “Dipole emitter”, Russian Patent 2 472 261, Date of filing: 10.08.2011, Date of publication: 10.01.2013.
12. D. A. Buhtiyarov et al., “Improvement of the quasi-Yagi antenna performances by using an ends-fed dipole driver”, *Universal J. Electr. Electron. Eng*., vol. 2, no. 1, 2014, pp. 6–17.
13. D. A. Buhtiyarov et al., “The linearly polarized waveguide-fed dipole-like antenna”, *J. Electromagn. Waves Appl*., vol. 29, no. 13, 2015, pp. 1720–1727. https://doi.org/10.1080/09205071.2015.1059293
14. S. A. Alekseytsev, A. P. Gorbachev, “The novel printed dual-band quasi-Yagi antenna with end-fed dipole-like driver”, *IEEE Trans. Antennas Propag*. vol. 68, no. 5, 2020, pp. 4088–4090.
15. M. Rafatullah, Editor. *Newest Updates in Physical Science Research*. London, Tarakeswar: BP Int, 2021, Volume 6, Chapter 8, https://doi.org/10.9734/bpi/nupsr/v6/2339F
16. A. M. Abbosh et al., “An UWB planar out-of-phase power divider employing microstrip-slot and parallel stripline-microstrip transitions”, *Proc. Asia-Pacific Microwave Conf*., 2006, vol. 1, pp. 905-908.
17. Price-list of the Company “SIBPROMISOLIT”, Kotelnikov’s Street, House no. 10, Room no. 41, Site Omsk, Omsk region, 644121, Russian Federation.
18. CST Studio Suite. Accessed: January 14, 2026, online. Available: http://www.cst.com/academia/student-edition.
19. K. Dzurinskyi, “Foreign and Russian radiofrequency connectors”, *Components and Technologies,* no. 2, 2011, pp. 38-43 (in Russian; available at www.kit-e.ru).
20. Z. Zhang et al., “Low-profile shared-structure dual-polarized Yagi-Uda antennas”, *IEEE Antennas and Wireless Propag. Lett*., vol. 21, no. 4, 2022, pp. 843–847. https://doi.org/10.1109/LAWP.2022.3150846
21. J. Lu et al., “Pattern reconfigurable Yagi antenna based on active corrugated stripline”, *IEEE Trans. Antennas Propag*., vol. 71, no. 1, 2023, pp. 1011–1016. https://doi.org/10.1109/TAP.2022.3215813
22. Y. Yin, K. Wu, “Endfire circularly polarized planar antennas: a review of their development”, *IEEE Antennas Propag. Mag*., vol. 65, no. 2, 2022, pp. 63–75. https://doi.org/10.1109/MAP.2022.3154977

23. A. K. Ospanova et al., “All-dielectric nanoantenna for efficient reflectors irradiation”, *Physical Sciences and Technology*, vol. 7, no. 1-2, 2020, pp. 25- 30. https://doi.org/10.26577/phst.2020.v7.i1.04

24. Q. Wang, et al., “Machine learning-assisted bandwidth optimization of quasi-Yagi antenna with adaptive dynamic parameter search range”, *IEEE Antennas and Wireless Propagation Letters*, vol. 25, no. 3, 2026, pp. 949 – 953.

Information about the authors:

Victor Atuchin (corresponding author) – Candidate of Physical and Mathematical Sciences, Professor, Research and Development Department, Kemerovo State University, Kemerovo, Russia; Laboratory of Optical Materials and Structures, Institute of Semiconductor Physics, SB RAS, Novosibirsk, Russia; Department of Industrial Machinery Design, Novosibirsk State Technical University (Novosibirsk 630073, Russia, e-mail: atuchin@isp.nsc.ru).

Dmitriy Buhtiyarov – Candidate of Technical Sciences, Researcher, Institute of Cosmic and Aviation Materials (NIICAM Co. Ltd.) Pereslavl-Zalessky, Russia, e-mail: ghostandfound@mail.ru;

Anatoly Gorbachev – Doctor of Technical Sciences, Professor, Radio Received and Transmitted Device Department, Novosibirsk State Technical University (Novosibirsk, Russia, e-mail: apgor1904@yandex.ru).

Vladimir Khrustalev – Doctor of Technical Sciences, Professor, General Physics Department, Novosibirsk State Technical University (Novosibirsk, Russia, e-mail: khrustalev@corp.nstu.ru).

Natalya Tarasenko – Candidate of Technical Sciences, Acting Associate Professor, General Physics Department, Novosibirsk State Technical University (Novosibirsk, Russia, e-mail: natalyavtarasenko@gmail.com).

Supporting materials

THE REDUCED SIZE QUASI-YAGI ANTENNA WITH AN ENDS-FED DIPOLE-LIKE DRIVER

First of all, the corresponding simulated current distributions on the surfaces of the modeled quasi-Yagi antenna at the selected three frequencies are presented in Figures S1-S3. These patterns confirm the proposed design based on the systematic parametric optimization.

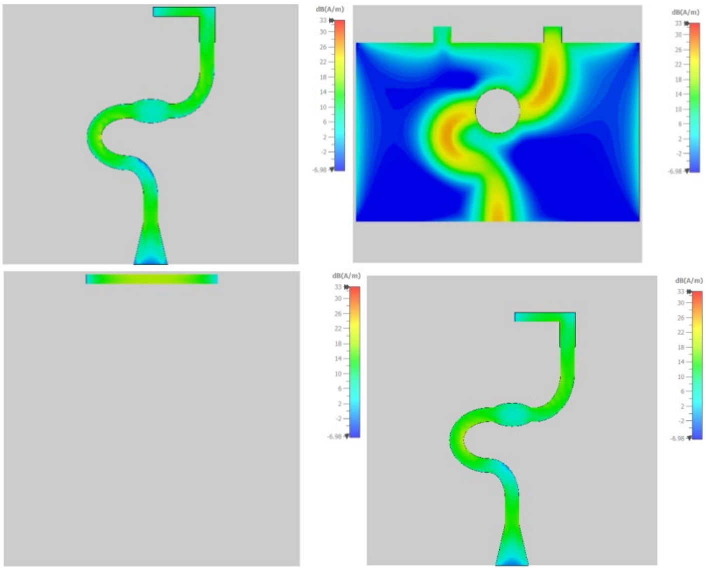

Figure S1. Simulated current distributions on the surfaces of all the layers at the frequency 2.55 GHz.

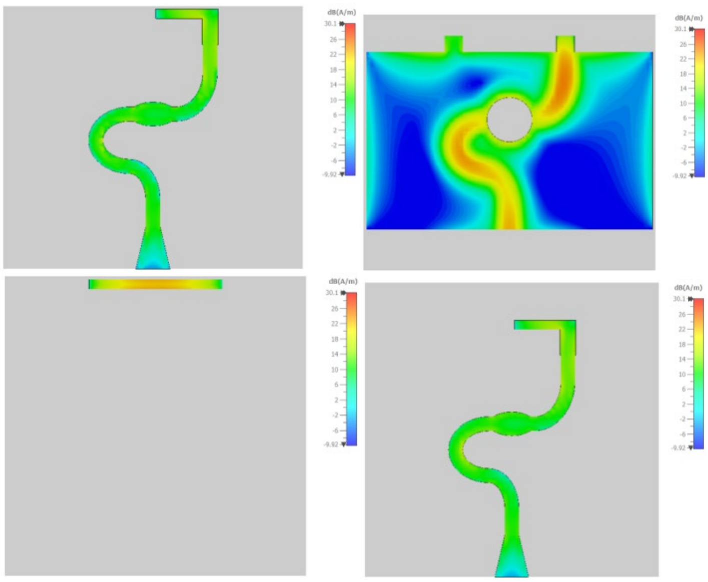

Figure S2. Simulated current distributions on the surfaces of all the layers at the frequency 2.8 GHz.

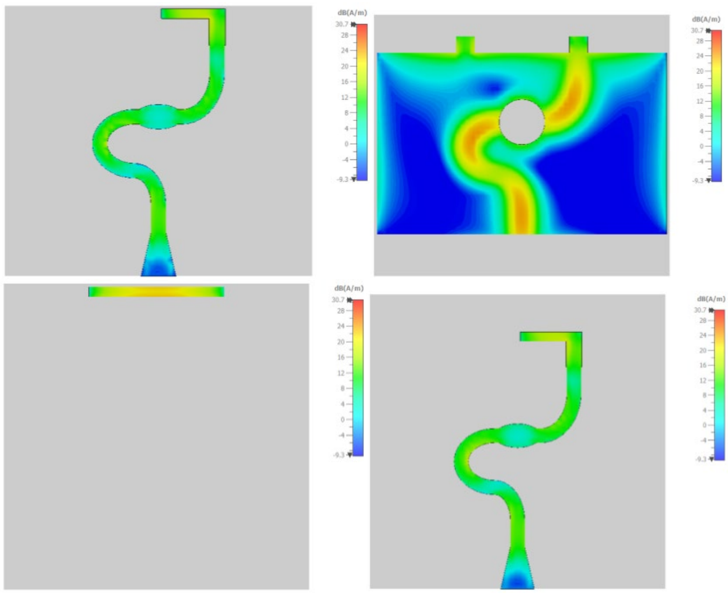

Figure S3. Simulated current distributions on the surfaces of all the layers at the frequency 3.05 GHz.

Secondly, to continue the analysis, the parametric studies are useful. Namely, Figure S4 displays the axis directions of the CST-model related to the proposed antenna whereas the little fragments inside Figure S5 represent the antenna topologies with additional designations by the letters related to following parametric studies.

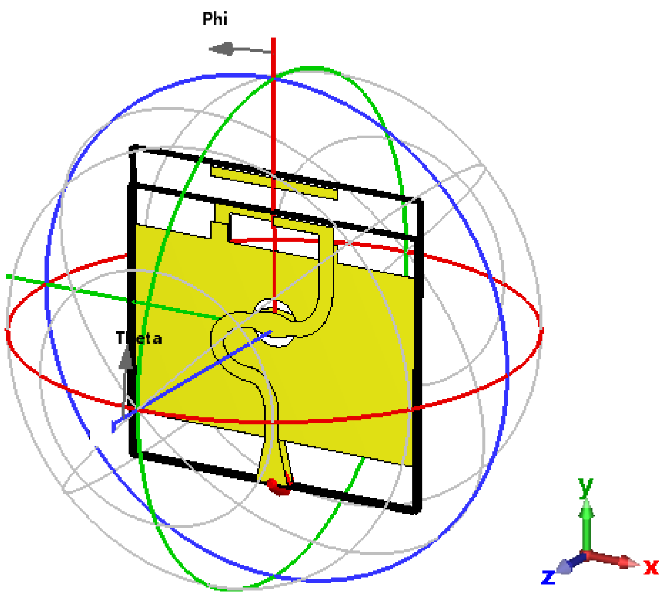

Figure S4. The axis directions of the antenna proposed.

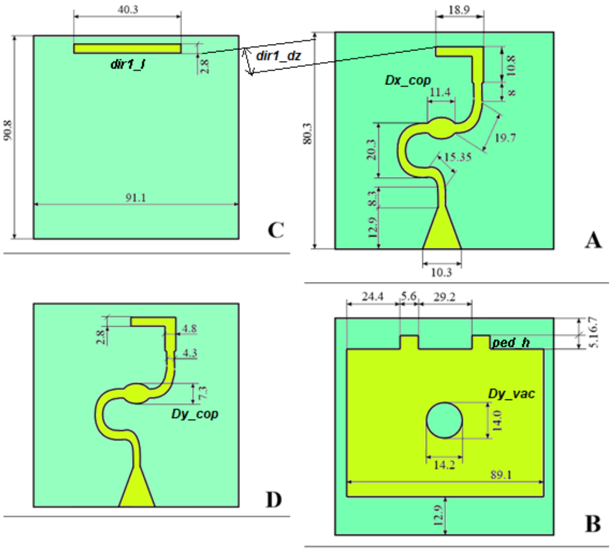

Figure S5. The antenna topologies with additional designations by the letters in order to display these values in the following Figures.

Now, Figures S6-S7 display the influences of the director length (dir1_l) on the input VSWR (Figure S6) and on the 2D co-polarized gain patterns in the E(xoy)-plane cut and in the H(zoy)-plane one (Figure S7).

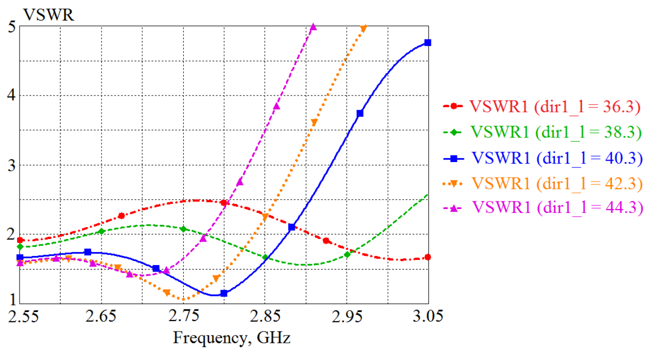

Figure S6. Input VSWR versus frequency with various director lengths (dir1_l).

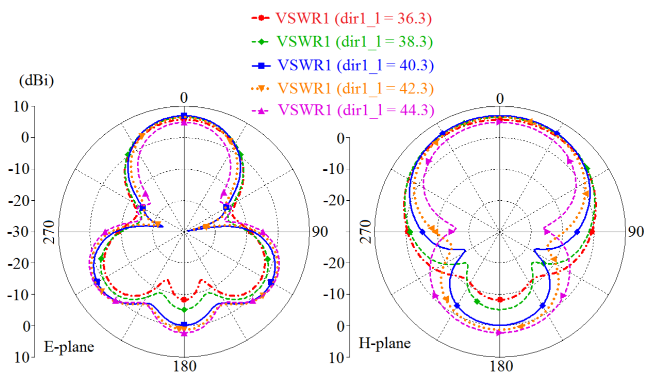

Figure S7. E- and H-plane co-polarized patterns versus the director length (dir1_l).

The following Figures S8-S9 present the influences of the distance (dir1_dz) between the director and the driver on the corresponding antenna performances when the value of the director length dir1_l is equal to 40.3 mm (blue curves in Figures S6-S7).

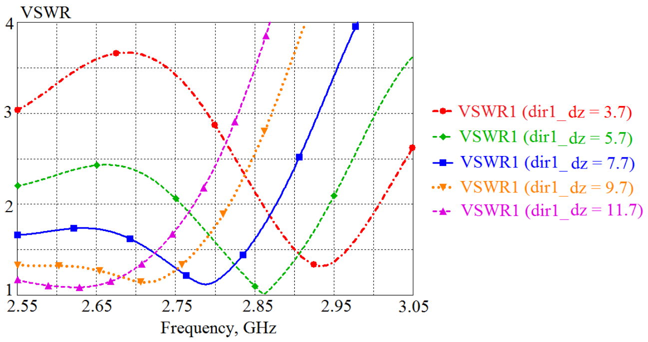

Figure S8. The input VSWR versus frequency
for various driver-to-director distances (dir1_dz).

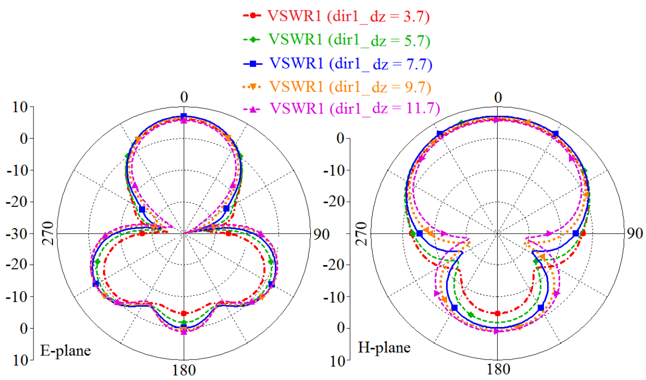

Figure S9. E- and H-plane co-polarized patterns
for various driver-to-director distances (dir1_dz).

Figures S10-S12 display the influences of the pedestal height (ped_h), of the vertical diameter (Dy_vac) of the hole, and of the vertical dimension (Dy_cop) of the elliptical patch on the input VSWR.

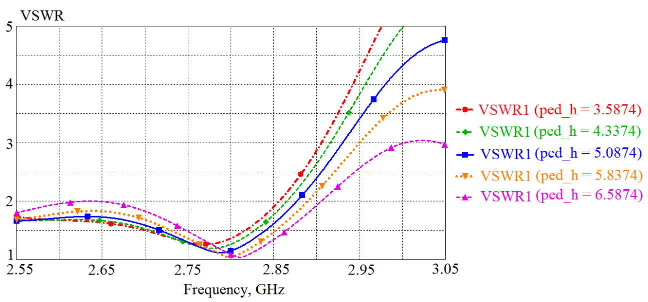

Figure S10. Input VSWR versus frequency
for various pedestal heights (ped_h).

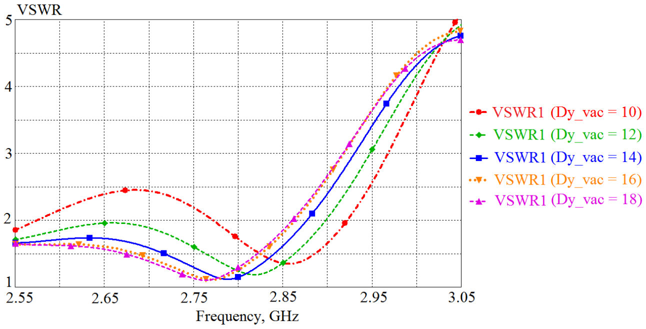

Figure S11. Input VSWR versus frequency
for various vertical diameters of the hole (Dy_vac).

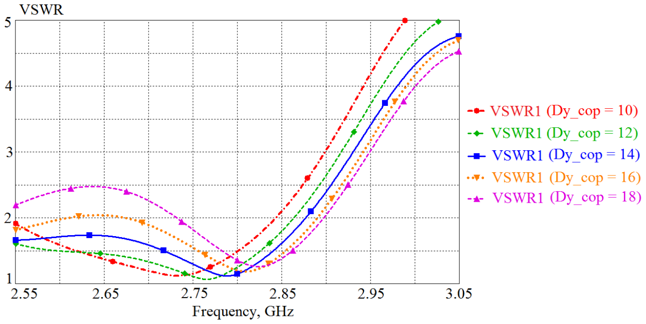

Figure S12. Input VSWR versus frequency
for various vertical dimensions of the elliptical patch (Dy_cop).

Thus, the parametric study confirms the proposed approach. Additionally, all the blue curves correspond to the optimum quantities of the quasi-Yagi antenna proposed.